Macromolecules

Article

pubs.acs.org/Macromolecules

Chain Overcrowding Induced Phase Separation and Hierarchical Structure Formation in Fluorinated Polyhedral Oligomeric Silsesquioxane (FPOSS)-Based Giant Surfactants

Xue-Hui Dong,[†] Bo Ni,[†] Mingjun Huang,[†] Chih-Hao Hsu,[†] Ziran Chen,[†] Zhiwei Lin,[†] Wen-Bin Zhang,*[,†,‡] An-Chang Shi,*[,§] and Stephen Z. D. Cheng*[,†]

[†]Department of Polymer Science, The University of Akron, Akron, Ohio 44325, United States

[‡]Key Laboratory of Polymer Chemistry and Physics of Ministry of Education, College of Chemistry and Molecular Engineering, Center for Soft Matter Science and Engineering, Peking University, Beijing 100871, China

[§]Department of Physics and Astronomy, McMaster University, Hamilton, Ontario L8S 4M1, Canada

Supporting Information

ABSTRACT: The self-assembly behaviors of fluorinated polyhedral oligomeric silsesquioxane (FPOSS)-based giant surfactants, consisting of an FPOSS cage and a polystyrene-*block*-poly(ethylene oxide) (PS-*b*-PEO) diblock copolymer tail, are studied in the bulk. The tethering point of the FPOSS cage on the PS-*b*-PEO diblock copolymer chain can be controlled precisely either at the end of the PS block or the junction point between the PS and PEO blocks, resulting in topological isomer pairs with almost identical chemical compositions but different architectures. Phase separation between the FPOSS head and the block copolymer tail creates a spatially confined environment for the PS-*b*-PEO component, which are uniformly end- or junction-point-immobilized on the FPOSS layer, providing a unique model system to study phase behaviors and chain conformation of tethered diblock copolymer in the condensed state. The polymer tails are highly stretched because the cross-sectional area of FPOSS head is smaller than that of the unperturbed block copolymer tail, which facilitates further phase separation between the low molecular weight PS and PEO blocks and leads to the formation of hierarchical lamellar structures among three mutually immiscible components.

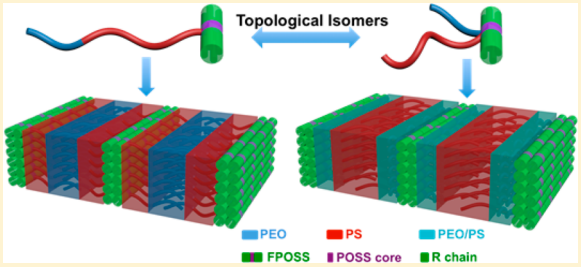

INTRODUCTION

Giant surfactants, as size-amplified counterpart of small-molecule surfactants, consist of compact and rigid molecular nanoparticles (MNPs) as head and flexible polymer chains as tail.[1,2] They capture the essential features of small-molecule surfactants yet with sizes comparable to block copolymers and therefore bridge the gap between these two classes of molecules.[1,2] Although computer simulations have predicted unconventional phase behaviors and abundant morphologies,[3−6] the self-assembly of these giant surfactants remains largely unexplored experimentally, mainly due to the lack of appropriate model systems with precisely defined molecular structures and topologies. Recently, we have designed and synthesized a series of giant surfactants based on functional MNPs,[1] e.g., [60]fullerene, polyhedral oligomeric silsesquioxane (POSS), and polyoxometalate derivatives, with variable surface functionalities and tunable topologies.[7−11] The phase behaviors of these giant surfactants possess a duality of both small-molecule surfactants and block copolymers.[7−10] They can self-assemble into a variety of ordered phases in the bulk which are similar to those found in flexible diblock copolymers[9] or micellar structures in solution with stretched polymer tails as observed in small-molecule surfactants.[7,8,10] The collective secondary interactions and geometric constraints of MNP heads result in highly diverse, thermodynamically stable or metastable nanostructures with feature sizes around or less than 10 nm.[1,9,12]

Introducing a second tail will greatly expand the scope of giant surfactants.[13,14] Depending on the tethering position of this second tail, i.e., at the end of the original tail or directly on the head, different molecular topologies could be obtained. These giant surfactants could be considered as *topological isomer pairs* if they possess similar chemical compositions. In the simplest case, the second tail has the same repeat units as the first one. We have elucidated the importance of molecular topology on the self-assembly behaviors of such topological isomers in previous reports.[8,9] For example, a bicontinuous double gyroid structure was observed in a giant surfactant with a hydroxyl-functionalized POSS (DPOSS) head and a single polystyrene (PS) tail (DPOSS-PS_{35}) in the bulk, while a hexagonal packed cylinder phase for the isomer with one DPOSS head and two PS tails (DPOSS-$2PS_{17}$, with the identical PS volume fraction).[9] A carboxylic acid-functionalized C_{60} (AC_{60}) tethered with one PS tail (AC_{60}-PS_{44}) formed

Received: July 26, 2015
Revised: September 14, 2015
Published: September 18, 2015

DOI: 10.1021/acs.macromol.5b01661
Macromolecules 2015, 48, 7172−7179

Scheme 1. Schematic Illustration and Chemical Structure of FPOSS-Based Giant Surfactants with FPOSS at the End of PS Block (FPOSS-PS-*b*-PEO, a) or at the Junction Point (PS-(FPOSS)-PEO, b)

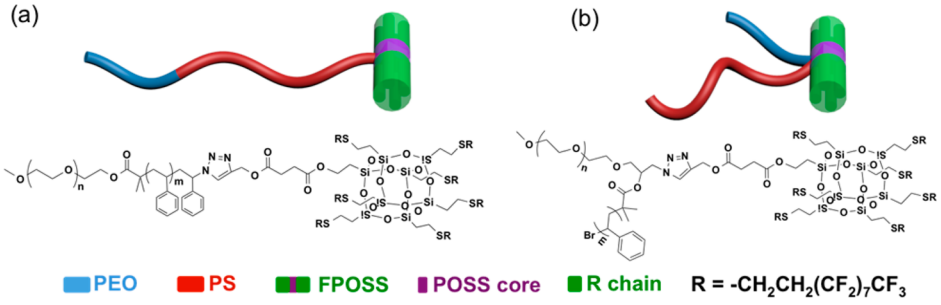

Table 1. Molecular Characterization of FPOSS-Based Giant Surfactants

sample[a]	M_w[b]	$M_{w,PS}$[c]	$M_{w,PEO}$[d]	$Đ$[e]	f[f]	*d*-spacing[g] d_1	*d*-spacing[g] d_2	$\tilde{\sigma}$[h]
1. FPOSS-PS_{28}-*b*-PEO_{45}	8800	2800	2000	1.10	0.31	14.5	13.5	3.8
2. FPOSS-PS_{48}-*b*-PEO_{45}	10800	4800	2000	1.08	0.24	16.8	14.7	5.2
3. FPOSS-PS_{64}-*b*-PEO_{45}	12400	6400	2000	1.06	0.20	17.2	15.1	6.5
4. PS_{23}-(FPOSS)-PEO_{45}	8300	2300	2000	1.10	0.33	10.8	11.0	1.7/1.6
5. PS_{38}-(FPOSS)-PEO_{45}	9800	3800	2000	1.08	0.27	12.6	13.0	1.7/2.6
6. PS_{54}-(FPOSS)-PEO_{45}	11400	5400	2000	1.09	0.23	13.6	12.3	1.7/3.8

[a]Sample label, the subscripts represent the degree of polymerization, *N*. [b]Overall molecular weight, in Da. [c]Molecular weight of PS, in Da, calculated based on ^{1}H NMR. [d]Molecular weight of PEO, in Da. [e]Polydispersity index, calculated based on SEC. [f]Volume fraction of FPOSS; see Supporting Information for detailed calculation. [g]Domain size below (d_1) and above (d_2) the melting temperature of FPOSS. [h]Reduced tethering density. For samples **4**–**6**, the first value refers to the reduced tethering density of the PEO block, while the second one refers to the PS block.

spherical micelles in solution, whereas the corresponding topological isomer with two tails (AC_{60}-$2PS_{23}$) formed vesicles under the same experimental conditions.[8]

On the other hand, introducing a second tail with chemically distinct repeating units could further promote the diversity and complexity of the self-assembled structures.[15−21] Giant surfactants with three mutually immiscible components or blocks are expected to generate multiple interactions, resulting in the formation of hierarchically structured morphologies.[14,22] To this end, we attached a 1*H*,1*H*,2*H*,2*H*-heptadecafluorodecyl-functionalized POSS (FPOSS) onto a polystyrene-*block*-poly(ethylene oxide) (PS-*b*-PEO) diblock copolymer at two specific positions: the end of the PS block (FPOSS-PS-*b*-PEO) or the junction point [PS-(FPOSS)-PEO] (Scheme 1).[14] We found that phase separation between the FPOSS heads and the PS-*b*-PEO tails uniformly immobilizes the block copolymer tails on the FPOSS layers at either the end of the PS block or the junction point. Although many theoretical and experimental studies have been carried out, a complete understanding of the phase behaviors of tethered block copolymers remains an outstanding challenge.[23−29] Most of the previous studies are based on surface-immobilized polymer thin film geometries.[23−25,27,28] The existence of air interfaces as well as limited film thickness makes the boundary conditions different from their bulk analogues. In this sense, these giant surfactants provide a unique model system for the investigation of the phase behaviors and chain conformation of tethered diblock copolymer in the bulk, where the interference of the air interface is eliminated. During structural formation the diblock copolymer tails are highly stretched because the cross-sectional area of the FPOSS head is smaller than that of unperturbed polymer tail. The chain-overcrowding leads to unexpected phase separation between the low molecular weight PS and PEO blocks and subsequent formation of hierarchical lamellar structures.

EXPERIMENTAL SECTION

Materials and Sample Preparation. The polymers were prepared through a combination of controlled/living radical polymerization and click chemistry. PS-*b*-PEO diblock copolymers with an azido functional group on either the chain-end or the junction point are synthesized by atom transfer radical polymerization (ATRP) with PEO macroinitiators. A "clickable" FPOSS is then attached onto the designated position on the block copolymer. All the giant surfactants have narrow molecular weight distributions (PDI < 1.10). The detailed syntheses, molecular analysis, and characterization can be found in our recent publication.[14] Uniform sample preparation procedure is applied to ensure the consistency of phase behaviors. Samples were annealed at 110 °C on a hot stage for 12 h under a N_2 atmosphere. All of the samples exhibit lamellar structure at nanometer scale.

Instrumentation and Characterizations. Small-angle X-ray scattering (SAXS) experiments were recorded on a Rigaku MicroMax 002+ instrument equipped with a high-intensity anode tube Cu X-ray generator. The typical working voltage and current for the X-ray source are 45 kV and 0.88 mA, respectively. The wavelength of beam is 0.154 nm. The signal was collected for 300 s by a CCD detector. Data were analyzed with the software SAXSgui provided by Rigaku. One-dimensional (1D) SAXS patterns were obtained by azimuthal integration of 2D patterns.

Two-dimensional (2D) wide-angle X-ray diffraction (WAXD) patterns were collected on a Rigakua instrument equipped with an 18 kW rotating anode X-ray generator in transmission mode. The wavelength of beam is 0.154 nm. The data were collected for 15 min with an R-AXIS-IV image plate detector. The peak positions were calibrated using silicon crystals. Background scattering from air was subtracted. One-dimensional (1D) WAXD patterns were obtained by azimuthal integration of 2D patterns.

Transmission electron microscopy (TEM) was recorded on JEOL 1200 EXII instrument. The accelerating voltage was 120 kV. Ultrathin specimens with 80−100 nm thickness were prepared by microtoming

DOI: 10.1021/acs.macromol.5b01661
Macromolecules 2015, 48, 7172−7179

the bulk sample using a Reichert Ultracut S (Leica) ultracryomicrotome machine at −30 °C. The specimen was directly observed or stained with RuO_4 vapor at room temperature for 10 min to increase contrast.

Differential scanning calorimetry (DSC) experiments were carried out using PerkinElmer PYRIS Diamond equipped with Intracooler 2P cooling system. The sample was prepared as described above and collected in a DSC alumina pan (typically ∼3 mg). The sample was sealed in the DSC pan and heated from 20 to 110 °C with a heating rate of 5 °C/min.

RESULTS AND DISCUSSION

Topological Isomer Pairs. Table 1 lists two categories of giant surfactants studied in this work. They can be regarded as topological isomer pairs on the basis of their almost identical chemical compositions and different architectures (for example, sample pairs of **1**/**4** and **2**/**6**). The degree of polymerization of the PEO block (N_{PEO}) is fixed to be 45, while the degree of polymerization of the PS block (N_{PS}) varies between 23 and 64. All of the samples exhibit lamellar structure at nanometer scale. Cylindrical and other hierarchical structures also form by tuning the composition. In the current work, we focus on the lamellar structure and leave the nonlamellar structures to future study.

Mesomorphic Nature of FPOSS. FPOSS is a unique type of building block due to the existence of fluoroalkyl side chains.[30−32] It is well-known that the fluoroalkyl chains adopt a rigid-rod-like conformation, which imparts a mesomorphic structure of the molecules.[33] There are two sets of diffraction peaks observed in one-dimensional (1D) small-angle X-ray scattering (SAXS) and wide-angle X-ray diffraction (WAXD) patterns of the FPOSS (Figure S1 in the Supporting Information). The peaks at low q range (0.18, 0.36, and 0.53 $Å^{-1}$) correspond to a lamellar structure with alternating POSS core and side chains, and the layer spacing is 3.5 nm ($d = 2\pi/q_1$). On the other hand, the peak at q = 1.28 $Å^{-1}$ comes from the packing of the 1*H*,1*H*,2*H*,2*H*-heptadecafluorodecyl chains, which characterizes the average distance between these rod-like molecules (0.49 nm).[34,35] It is close to the interstem distance of the polytetrafluoroethylene (PTFE) crystal that has the closest hexagonal packing of fluoroalkyl chains (0.49 nm).[35,36] These two sets of peaks orientated perpendicularly to each other, as revealed by the 2D WAXD pattern with sheared samples (Figure S1c). No diffractions are observed in the quadrants. The FPOSS thus adopts a mesomorphic packing, with the long axis perpendicular to the layer and the 1*H*,1*H*,2*H*,2*H*-heptadecafluorodecyl rods are hexagonally packed within the layer (Figure S1d). Similar structures have also been observed in the polymers with pendant fluoroalkyl side chains.[34,35,37,38] The layer spacing (3.5 nm) is about twice of the length of the 1*H*,1*H*,2*H*,2*H*-heptadecafluorodecyl rods, indicating a double-layered arrangement rather than interdigitated.[34,35] Based on these characterizations, the FPOSS can be regarded as a cylinder with a diameter of ∼1 nm and a height of 3.5 nm, considering that there are four fluoroalkyl chains on each side (Figure S1d). The FPOSS mesomorphic phase has a transition to the isotropic melt at the temperature (T_i) of 88 °C (Figure S2a). Note that this transition temperature is depressed to 50 °C (Figure S2b) after conjugating with PS-*b*-PEO block copolymers.

Identification of the Hierarchical Structures. Figures 1a and 1b show the SAXS and WAXD patterns of sample **1** (FPOSS-PS_{28}-*b*-PEO_{45}, Table 1). Two sets of diffraction peaks are observed, revealing the existence of hierarchically ordered

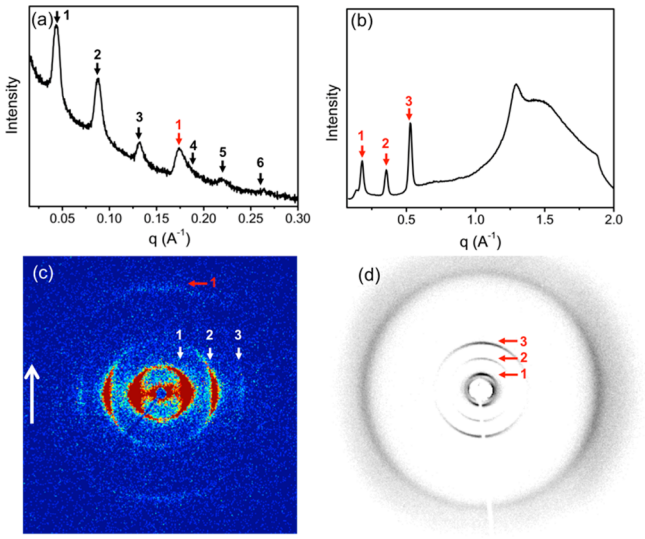

Figure 1. 1D SAXS (a) and WAXD (b) patterns of sample **1** (FPOSS-PS_{28}-*b*-PEO_{45}) at room temperature. The sample was mechanically sheared and then characterized by 2D SAXS (c) and WAXD (d). The arrow in (c) represents shear direction.

structures within two length scales. First of all, the SAXS peaks in low q region (black arrows in Figure 1a) with a q/q_1 ratio of 1:2:3:4:5:6 indicate a lamellar structure, presumably induced by nanophase separation between the FPOSS head and the PS-*b*-PEO tail, with a domain period d = 14.5 nm. The domain sizes vary with the molecular weights of the block copolymer tails (Table 1). In addition, there is another set of diffraction peaks with primary diffraction (q_1') at 0.18 nm^{-1} and the q/q_1' ratio of 1:2:3 (red arrows in Figures 1a and 1b), corresponding to another lamellar structure with a much smaller domain spacing d' = 3.5 nm. The positions of this set of diffractions are independent of the length of block copolymer tails and in good agreement with the X-ray diffraction patterns of the pure FPOSS MNPs (Figure S1). It can thus be concluded that the second lamellar structure originates from the mesomorphic packing in the FPOSS domain, with alternating silicon−oxygen frame and fluoroalkyal rods.[31] The PEO blocks are not crystallized due to their low molecular weight (Figure 1b).

In order to identify the orientation relationship between these two lamellar structures, the samples were mechanically sheared and characterized by 2D SAXS and WAXD (Figures 1c and 1d). The shear direction is along the meridian direction as indicated by the arrow in Figure 1c. It is evident that these two sets of arcs are in orthogonal orientations. The arcs on the equator correspond to the larger lamellar structure (lamellae with alternating FPOSS and block copolymer domains), and its normal direction is perpendicular to the shear direction (Figure 1c). The arcs on the meridian, on the other hand, are attributed to the lamellar structure within the FPOSS domains, of which the normal direction is parallel to the shear direction.

The ordered structure deduced from the scattering results is confirmed by bright-field (BF) transmission electron microscopy (TEM) images in real space. Figure 2a shows a highly asymmetric lamellar pattern of sample **1** with alternating dark and light layers. The overall domain period is estimated to be 15 nm, consistent with the calculated size of the first lamellar structure based on the SAXS result (14.5 nm). The dark layer with a width of ∼3 nm is the FPOSS domain due to its higher electron density, while the light layer (∼12 nm) corresponds to

DOI: 10.1021/acs.macromol.5b01661
Macromolecules 2015, 48, 7172−7179

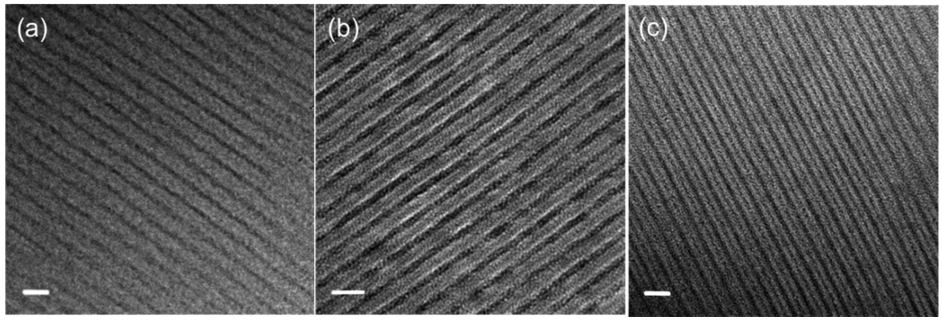

Figure 2. Bright-field TEM images of sample **1** (FPOSS-PS_{28}-*b*-PEO_{45}) before (a) and after (b) RuO_4 staining. Stained image of sample **2** (FPOSS-PS_{48}-*b*-PEO_{45}) is shown in (c) as comparison. The scale bar is 20 nm.

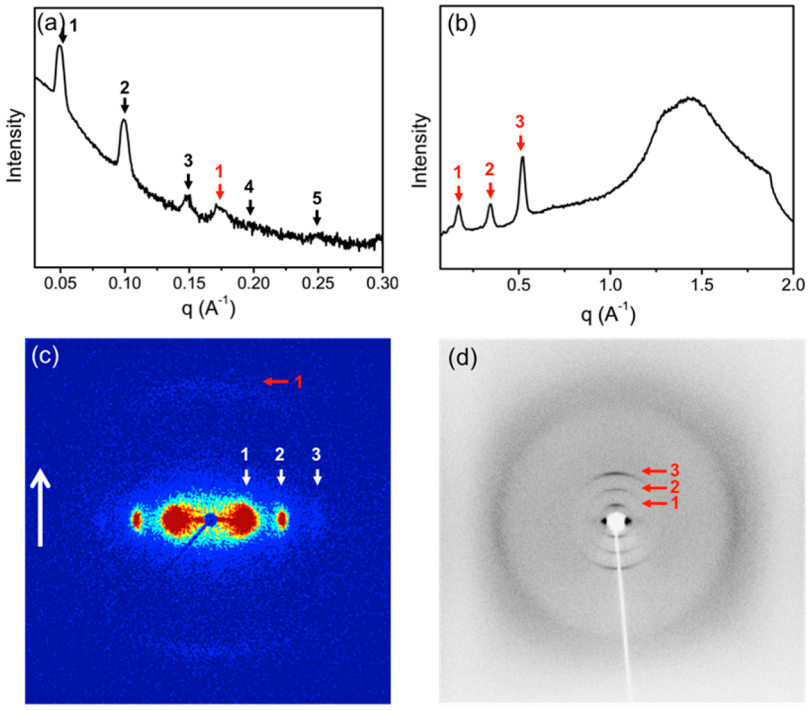

Figure 3. 1D SAXS (a) and WAXD (b) patterns of sample **5** (PS_{38}-(FPOSS)-PEO_{45}) at room temperature. The sample was then mechanically sheared and characterized by 2D SAXS (c) and WAXD (d). The arrow in (c) represents shear direction.

the PS-*b*-PEO domain.[31] The lamellar structure within the FPOSS domain is not visible under the resolution of TEM experiment. The highly asymmetric domain size may imply an unusual molecular arrangement of the PS-*b*-PEO tails within the polymer domain.

In order to explore the internal structure, a RuO_4-stained sample **1** was examined by TEM (Figure 2b). As compared to unstained image (Figure 2a), additional dark layers appear at the center of the polymer domains. Since PEO is more reductive than PS, it is more readily stained by RuO_4,[39] making the PEO blocks darker than the FPOSS domain (which now becomes gray). The light layers between them are the PS domains. This assignment is consistent with geometrical connection (Scheme 1a) and can be further confirmed by varying the molecular weights of the PS blocks. The TEM image of RuO_4-stained sample **2** (FPOSS-PS_{48}-*b*-PEO_{45}) is shown in Figure 2c. With increasing PS block length, the width of the PS domain (the light layers) increases as compared to **1** (Figure 2b). From these observations it can be concluded that the PS-*b*-PEO undergoes nanophase separation within the polymer domain, forming alternating and parallel FPOSS/PS/PEO/PS/FPOSS layers.

It should be noted that for a flexible block copolymer such as PS-*b*-PEO phase separation occurs when the enthalpy change overcomes the entropic penalty. For a symmetric diblock copolymer, mean-field theory predicts a critical immiscibility between two blocks ($\chi N > 10.5$).[40,41] The relatively weak interaction between PS and PEO blocks ($\chi \sim 0.08$) implies that phase separation of PS-*b*-PEO block copolymer could only take place when N is sufficiently large ($N > 130$).[42] A much higher N is required to form ordered structures with sharp interfaces (experientially, $N \sim 300$).[42] The molecular weights of the PS-*b*-PEO diblock copolymer tails involved in this study are much lower than the limit, which should remain in a disordered state. It is therefore highly unexpected that phase separation between the PS and PEO blocks occurs in these FPOSS-based giant surfactants.

A parallel study of the hierarchical structure of PS-(FPOSS)-PEO reveals importance of the molecular topology on the self-assembly behaviors. In this class of giant surfactants, the FPOSS is tethered at the junction point between the PS and PEO

DOI: 10.1021/acs.macromol.5b01661
Macromolecules 2015, 48, 7172−7179

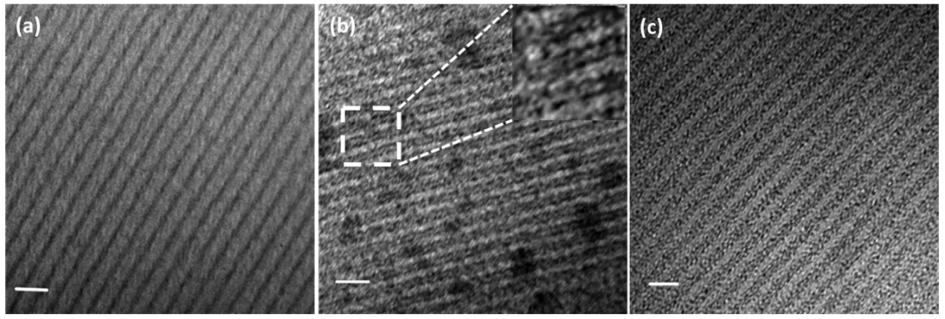

Figure 4. TEM bright-field images of sample **5** (PS_{38}-(FPOSS)-PEO_{45}) before (a) and after (b) RuO_4 staining. Stained image of sample **6** (PS_{54}-(FPOSS)-PEO_{45}) is shown in (c) as comparison. The scale bar is 20 nm.

blocks, resulting in two chemically distinct tails.[13] Two sets of diffraction peaks in 1D SAXS and WAXD patterns with both q/q_1 ratio of 1:2:3... are also observed (sample **5**, Figures 3a and 3b), indicating the existence of two independent lamellar structures. Similarly, the first set of diffraction peaks can be assigned to the lamellae between the FPOSS heads and the copolymer tails (Figure 3a, black arrows, d = 12.5 nm), while the second set (Figures 3a and 3b, red arrows) is attributed to the layer structure within the FPOSS domain. The orthogonal orientation of these two lamellae can also be elucidated by 2D SAXS and WAXD experiments utilizing mechanically sheared sample (Figures 3c and 3d). The diffraction arcs corresponding to the first lamellae locate on the equator, while the second set on the meridian.

A bright-field TEM image of sample **5** (Figure 4a) also shows alternating dark (the FPOSS domain, ~3 nm) and light (the PS/PEO domain, ~10 nm) layers. The overall domain period is estimated to be 13 nm, consistent with the SAXS result (12.5 nm, Figure 3a). Note that sample **5** possesses a longer PS block (N_{PS} = 38) but a smaller domain spacing compared with sample **1** (N_{PS} = 28, d = 14.5 nm), indicating that the topological effect must lead to different molecular packing during structural formation.

A bright-field TEM image of RuO_4-stained sample **5** is shown in Figure 4b. The morphology differs from the unstained image (Figure 4a) in two aspects. First, the width of the dark layer increases while the overall domain period keeps constant, and second, the dark layer consists of a sandwiched structure with a middle gray domain (Figure 4b, inset). These observations indicate that the PS and PEO blocks are again nanophase separated. An multilayer lamellar structure can be identified in a sequence of FPOSS (gray)/(PEO/PS) (dark)/PS (light)/(PS/PEO) (dark)/FPOSS (gray). Because of molecular geometrical constraint, the PS blocks have to penetrate out of the PEO domains with relatively extended conformations, while the PEO blocks appear to collapse near the FPOSS layers. This proposed PS/PEO arrangement can be confirmed by varying the length of the PS block tails. Indeed, an increased width of the PS domain was observed in sample **6** with higher PS molecular weight (Figure 4c).

Based on the X-ray diffraction and TEM results and molecular architectures, detailed molecular arrangements in the hierarchical structures are established (Scheme 2). In both cases, phase separation between the FPOSS head and the block copolymer tail creates the primary lamellar frame composed of alternating FPOSS and PS/PEO domains. At a smaller length scale, phase separation between the PS and PEO blocks takes place in the polymer domains while segregation of silicon–oxygen core and fluoroalkyl side chains occurs in the FPOSS domains. The combination of these processes leads to the formation of hierarchically ordered structures observed in the experiments. In the direction along the copolymer tail, the multilayered nanostructures exhibit different layer sequences, i.e., FPOSS/PS/PEO/PS/FPOSS for the linear FPOSS-PS-*b*-PEO (Scheme 2a) whereas FPOSS/(PEO/PS)/PS/(PS/PEO)/FPOSS for the star-like PS-(FPOSS)-PEO (Scheme 2b). In the perpendicular direction, alternating arrangement of the POSS core and fluoroalkyl chain constructs another lamellar structure within the FPOSS domain. The phase separation between the PS and PEO blocks is not revealed in the SAXS patterns since the electron density difference between amorphous PS and PEO is much smaller than that between the PS/PEO and the FPOSS.[31,43]

Scheme 2. Schematic Illustration of Hierarchical Structures of FPOSS-PS-*b*-PEO (a) and PS-(FPOSS)-PEO (b)

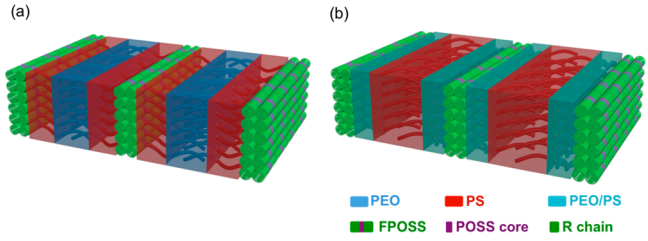

Stretching of Polymer Tails. The thickness of the PS-*b*-PEO domain of sample **1** (light layer in Figure 2a) is about 12 nm, which is significantly larger than the unperturbed size of the PS_{28}-*b*-PEO_{45} diblock copolymers (identical to the tail part of sample **1**) in its melt state. In fact, it also exceeds the estimated domain period of PS_{28}-*b*-PEO_{45} diblock copolymer assuming it could form lamellar structure. As a reference, PS_{92}-*b*-PEO_{200} diblock copolymer with a similar composition, but a molecular weight about ~4 times larger, has been observed to form a lamellar structure with d = 18.7 nm.[42] For lamellae in the strong segregation limit, the relationship between d and N follows the scaling law, $d \sim N^{2/3}$.[44] The d of PS_{28}-*b*-PEO_{45} could thus be extrapolated to be 7.8 nm. This value can only be viewed as an upper limit, since the blocks in the current case are with low molecular weight and not in the strong segregation regime. The extrapolated domain spacing (7.8 nm) is certainly much smaller than the experimentally observed one (~12 nm). This large domain spacing reveals that the block copolymer tails in the giant surfactants must be heavily stretched.

The chain stretching can be experimentally confirmed by temperature-dependent SAXS, as shown in Figure 5a. A sudden decrease of the overall lamellar period from 14.5 to 13.5 nm is

DOI: 10.1021/acs.macromol.5b01661
Macromolecules 2015, 48, 7172–7179

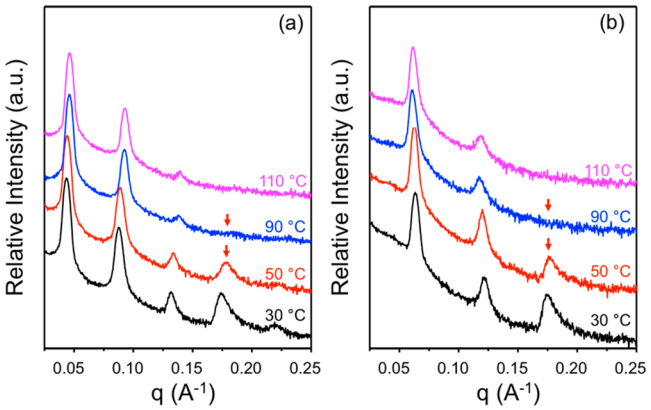

Figure 5. Temperature-dependent SAXS patterns of sample **1** (FPOSS-PS_{28}-*b*-PEO_{45}, a) and sample **4** (PS_{23}-(FPOSS)-PEO_{45}, b).

observed when heating sample **1** to above the transition temperature (50 °C, Figure S2b), accompanied by the disappearance of the WAXD diffractions of the FPOSS mesomorphic phase (red arrows in Figure 5a). Further increasing the temperature does not lead to appreciable change of the domain spacing. Considering that a slight increase of domain spacing is expected upon heating, the observed sudden shrinkage of the lamellar period *d* can be reasonably explained by the release of chain stretching of polymer tails.

The strong stretching of the PS-*b*-PEO chains is attributed to the overcrowding of the diblock copolymer tails in confined environments. Upon phase separation, the PS-*b*-PEO tails will be tethered onto the FPOSS "substrate", resulting in a high grafting density. The mesomorphic FPOSS has a fixed volume and shape and thus provides a defined cross-sectional area for each tethered copolymer tail. Qualitatively, the polymer tails can be viewed as being confined in a rectangle nanochannel with a cross-sectional area smaller than the size of the unperturbed block copolymer tails, which leads to the chain stretching. The reducing tethering density ($\tilde{\sigma}$), which characterizes the chain overcrowding, can be quantitatively calculated.[45] The onset of chain overcrowding occurs at $\tilde{\sigma}$ = 3.7.[45,46] At this point, the tethered chains start to feel their neighbors and deviate from the unperturbed state. For sample **1**, the reducing tethered density of PS_{28}-*b*-PEO_{45} tail is estimated to be about 3.8 (see Supporting Information for detailed calculation). This value enters the regime where tethered polymer tails are stretched.[45,46] Further increasing the tail molecular weight increases $\tilde{\sigma}$ and leads to a stronger stretching of the tail to accommodate the cross-sectional area provided by the corresponding FPOSS head. This can be confirmed by a comparison of the samples with different tail length (Table 1). A larger shrinkage upon heating is observed for sample **2** with higher tail molecular weight (d_1 = 16.8 nm, d_2 = 14.7 nm; see Table 1) as compared to sample **1** (d_1 = 14.5 nm, d_2 = 13.5 nm). It should be noted that the expansion of cross-sectional area of FPOSS during melting could only partially release the stretching of polymer chain since the primary lamellar structure retains (Figure 5). The width of polymer domain of sample **1** above 50 °C (~10 nm) is still larger than the expected lamellar domain size (7.8 nm).

A quite different molecular packing is found in the case of PS-(FPOSS)-PEO. For samples **4** and **5** with similar overall molecular weight as sample **1**, no decrease of the lamellae period is observed upon heating (Figure 5b and Table 1). The shrinkage occurs at much higher molecular weight of the PS block (**6**, see Table 1). In this case, two homopolymer tails, instead of a single long copolymer tail, are tethered to the same position on the FPOSS "substrate". In principle, this molecular geometry should lead to even more severe chain overcrowding because grafting density are doubled. It should be noted that the calculation of reduced tethering density is based on the assumption that the PS and PEO blocks are in an unperturbed disordered state. There are two possibilities to alleviate the chain overcrowding: both the PS and PEO blocks stretch out in the direction along the normal of the FPOSS layer, or one block suffers from stretching while the other collapses onto the "substrate". The structural analysis in previous section indicates the latter case is close to the experimental observation. The tethering density should thus be considered separately. The reduced tethering density of PEO ($\tilde{\sigma}_{PEO}$) is calculated to be 1.7 (see Supporting Information), which is below the onset of overcrowding. The PEO tails somewhat collapse (Scheme 2) and can be confirmed by the small domain size of the PEO layer in the TEM images (Figure 4b). On the other hand, the reduced tethering density of PS ($\tilde{\sigma}_{PS}$) is listed in Table 1 (also see Supporting Information). No chain overcrowding was observed until the N_{PS} reaches 54 (sample **6**, $\tilde{\sigma}_{PS}$ = 3.8). The difference between the chain conformations of these two topological isomers clearly highlights the importance of the molecular geometry.

Enhanced Immiscibility Due to Confinement. Thermodynamically, two competing free energy contributions determine the structural formation of diblock copolymer in the isotropic bulk: the enthalpic gain due to decrease of interface area and the entropic loss due to chain stretching and localization of junction points at interface.[40,47] Considering the relatively weak interaction between PS and PEO blocks,[43] the gain of the enthalpic interactions cannot compensate the entropic penalty for low molecular weight PS-*b*-PEO diblock copolymers (with similar molecular weight as the tails involved in this study), and therefore phase separation is not supposed to occur. In order to understand the observed microphase separation between the PS and PEO blocks in our system, the formation of the hierarchical structures could be divided into two processes taking place in tandem. The strong repulsion between the FPOSS cages and the polymer tails first leads to the formation of the primary lamellar frame. Phase separation of the PS and PEO blocks then occurs in the polymer domain sandwiched between two neighboring FPOSS domains. The pre-existing FPOSS lamellae must exert additional driving forces on the phase separation of the polymer tails. Different from diblock copolymers in their melt state, the tethered PS-*b*-PEO tails have two unique characteristics: their ends (or junction points) are uniformly grafted on a flat lamellar substrate, and each chain is stretched to fit the space as in the polymer brush systems. The strongly stretched chain could be viewed as approximately confined in a nanochannel with a cross-sectional area defined by the size of the FPOSS head if the overlap of the neighboring polymer chains is ignored according to the Alexander–de Gennes model.[48−51] The conformation of a stretched polymer chain is strongly altered as compared with the melt state. For polymer chains confined in a nanotube, it has been demonstrated that entropic contribution due to stretching of the chains provides a driving force for different polymers to separate from each other.[52] In the case of the current system, the PS-*b*-PEO chains form a brush on the surface of the FPOSS lamellae. The afore-

DOI: 10.1021/acs.macromol.5b01661
Macromolecules 2015, 48, 7172−7179

mentioned entropic driving force provides an additional driving force for the PS/PEO phase separation.

In the case of FPOSS-PS-*b*-PEO, the PS and PEO blocks undergo nanophase separation due to covalent connection. It is natural to have the PS block starting at the tethering point, followed by the PEO block. The cross-sectional area provided by FPOSS head cannot accommodate the corresponding polymer tails. The stretched polymer chain is impossible to retreat back to form disordered mixture due to steric hindrance. This scenario can also be interpreted in the following way. Formation of ordered structures accompanies by an entropy loss since the possible configurations will be depressed as compared with the initial disordered states.[40,47] The decrease of entropy during phase separation can be understood in two parts: configurational entropy loss due to chain stretching and translational entropy loss due to localization of tethering points at the interface.[41] Immobilization of chain ends reduces translational entropy penalty by depressing initial possible configurations, which has been reported to promote phase separation.[53] However, it is usually negligible.[41] The loss of configurational entropy due to chain stretching is thus the major barrier that hampers phase separation. For FPOSS-PS-*b*-PEO, the PS-*b*-PEO block copolymer tails have already been stretched to an extent that even exceeds the requirement of lamellar formation. Under this circumstance, no additional entropy penalty is required for phase separation. The overall free energy is dominated by enthalpy, and phase separation is favored to minimize the contact between two blocks.

Upon heating, the tethered PS-*b*-PEO diblock copolymers slightly retreat back to release the excess chain stretching imposed by the FPOSS (from mesomorphic packing to isotropic). It is worth noting that the phase separation between the low molecular weight PS and PEO blocks is in the strong segregation regime, and no order−disorder transition was observed even at 180 °C. It can be confirmed by the TEM image of specimen quenched from high temperatures to liquid nitrogen (Figure S3, which also rules out the possibility that phase separation is due to crystallization of PEO block). Though the degree of stretching has been partially released when the FPOSS becomes isotropic (Figure 5a), the confinement does not break down since the overall lamellar structure between FPOSS head and block copolymer retains. The phase separation between the PS and PEO blocks always take places even we push the N to the lower limit of controlled/living radical polymerization, which exactly follows the prediction of the blob-scaling approach.

In the case of PS-(FPOSS)-PEO, the interface between the PS and PEO domain no longer coincides with the junction point between these two blocks because both of them are forced to locate in the same side of the junction point. A simple model for this case is that two polymer chains (PS and PEO) are tethered at the end of the confining cylinder. There are two possible configurations: both of the chains stretching out to form a mixed structure, or two chains phase separate and occupy different sections of the cylinder. Under the latter circumstance, one chain has to stretch out while the other collapse, which maximizes the chain configuration entropy and minimizes the PS/PEO interactions. According to the scaling argument mentioned above, entropy would drive the two polymers to segregate. The PS/PEO interaction energy will provide further driving force for phase separation. We thus expect that phase separation between low molecular weight PS and PEO blocks would also occur in this category of samples. Although there is a short portion of the PS block embedded in the PEO layer, the energy cost could be compensated by the total free energy gain due to the PS/PEO separation.

CONCLUSIONS

In summary, the self-assembly behaviors of an FPOSS-based topological isomer pair are studied. Hierarchical lamellar structures are observed in both cases. Phase separation between the FPOSS head and the copolymer tail leads to the formation of a primary lamellar frame with alternating FPOSS and PS/PEO layers. Further segregation of the PS and PEO blocks in polymer domain and the silicon−oxygen core and fluoroalkyl side chains in FPOSS domain results in secondary lamellar structures with smaller length scales. Polymer tails are uniformly tethered onto FPOSS layer and highly stretched due to the confinement, providing an additional driving force toward phase separation of low molecular weight PS and PEO blocks. This study clearly illustrates the importance of molecular geometry on the self-assembly. It provides a unique model system to study the phase behaviors and chain conformation of tethered block copolymers in the condensed state.

ASSOCIATED CONTENT

Supporting Information

The Supporting Information is available free of charge on the ACS Publications website at DOI: 10.1021/acs.macromol.5b01661.

Detailed experimental procedures and additional characterizations (PDF)

AUTHOR INFORMATION

Corresponding Authors

*E-mail scheng@uakron.edu (S.Z.D.C.).
*E-mail shi@mcmaster.ca (A.-C.S.).
*E-mail wenbin@pku.edu.cn (W.-B.Z.).

Notes

The authors declare no competing financial interest.

ACKNOWLEDGMENTS

This work was supported by National Science Foundation (DMR-1409972). A.-C.S. acknowledges the support by the Natural Science and Engineering Research Council of Canada.

REFERENCES

(1) Zhang, W.-B.; Yu, X.; Wang, C.-L.; Sun, H.-J.; Hsieh, I.-F.; Li, Y.; Dong, X.-H.; Yue, K.; Van Horn, R.; Cheng, S. Z. D. *Macromolecules* **2014**, *47*, 1221.
(2) Yu, X.; Li, Y.; Dong, X.-H.; Yue, K.; Lin, Z.; Feng, X.; Huang, M.; Zhang, W.-B.; Cheng, S. Z. D. *J. Polym. Sci., Part B: Polym. Phys.* **2014**, *52*, 1309.
(3) Glotzer, S. C.; Horsch, M. A.; Iacovella, C. R.; Zhang, Z.; Chan, E. R.; Zhang, X. *Curr. Opin. Colloid Interface Sci.* **2005**, *10*, 287.
(4) Horsch, M.; Zhang, Z.; Glotzer, S. *Phys. Rev. Lett.* **2005**, *95*, 056105.
(5) Glotzer, S. C.; Solomon, M. J. *Nat. Mater.* **2007**, *6*, 557.
(6) Zhu, X.; Wang, L.; Lin, J.; Zhang, L. *ACS Nano* **2010**, *4*, 4979.
(7) Yu, X.; Zhong, S.; Li, X.; Tu, Y.; Yang, S.; Van Horn, R. M.; Ni, C.; Pochan, D. J.; Quirk, R. P.; Wesdemiotis, C.; Zhang, W.-B.; Cheng, S. Z. D. *J. Am. Chem. Soc.* **2010**, *132*, 16741.
(8) Yu, X.; Zhang, W. B.; Yue, K.; Li, X.; Liu, H.; Xin, Y.; Wang, C. L.; Wesdemiotis, C.; Cheng, S. Z. D. *J. Am. Chem. Soc.* **2012**, *134*, 7780.

DOI: 10.1021/acs.macromol.5b01661
Macromolecules 2015, 48, 7172−7179

(9) Yu, X.; Yue, K.; Hsieh, I. F.; Li, Y.; Dong, X. H.; Liu, C.; Xin, Y.; Wang, H. F.; Shi, A. C.; Newkome, G. R.; Ho, R. M.; Chen, E. Q.; Zhang, W. B.; Cheng, S. Z. D. *Proc. Natl. Acad. Sci. U. S. A.* **2013**, *110*, 10078.
(10) Wang, Z.; Li, Y.; Dong, X.-H.; Yu, X.; Guo, K.; Su, H.; Yue, K.; Wesdemiotis, C.; Cheng, S. Z. D.; Zhang, W.-B. *Chem. Sci.* **2013**, *4*, 1345.
(11) Dong, X.-H.; Zhang, W.-B.; Li, Y.; Huang, M.; Zhang, S.; Quirk, R. P.; Cheng, S. Z. D. *Polym. Chem.* **2012**, *3*, 124.
(12) Huang, M.; Hsu, C.-H.; Wang, J.; Mei, S.; Dong, X.; Li, Y.; Li, M.; Liu, H.; Zhang, W.; Aida, T.; Zhang, W.-B.; Yue, K.; Cheng, S. Z. D. *Science* **2015**, *348*, 424.
(13) Li, Y.; Dong, X.-H.; Guo, K.; Wang, Z.; Chen, Z.; Wesdemiotis, C.; Quirk, R. P.; Zhang, W.-B.; Cheng, S. Z. D. *ACS Macro Lett.* **2012**, *1*, 834.
(14) Ni, B.; Dong, X.-H.; Chen, Z.; Lin, Z.; Li, Y.; Huang, M.; Fu, Q.; Cheng, S. Z. D.; Zhang, W.-B. *Polym. Chem.* **2014**, *5*, 3588.
(15) Bates, F. S.; Hillmyer, M. A.; Lodge, T. P.; Bates, C. M.; Delaney, K. T.; Fredrickson, G. H. *Science* **2012**, *336*, 434.
(16) Mogi, Y.; Mori, K.; Matsushita, Y.; Noda, I. *Macromolecules* **1992**, *25*, 5412.
(17) Auschra, C.; Stadler, R. *Macromolecules* **1993**, *26*, 2171.
(18) Gido, S. P.; Schwark, D. W.; Thomas, E. L. *Macromolecules* **1993**, *26*, 2636.
(19) Krappe, U.; Stadler, R.; Voigt-Martin, I. *Macromolecules* **1995**, *28*, 4558.
(20) Bailey, T. S.; Pham, H. D.; Bates, F. S. *Macromolecules* **2001**, *34*, 6994.
(21) Bailey, T. S.; Hardy, C. M.; Epps, T. H.; Bates, F. S. *Macromolecules* **2002**, *35*, 7007.
(22) He, J.; Yue, K.; Liu, Y.; Yu, X.; Ni, P.; Cavicchi, K. A.; Quirk, R. P.; Chen, E.-Q.; Cheng, S. Z. D.; Zhang, W.-B. *Polym. Chem.* **2012**, *3*, 2112.
(23) Milner, S. T. *Science* **1991**, *251*, 905.
(24) Zhao, B.; Brittain, W. J. *Prog. Polym. Sci.* **2000**, *25*, 677.
(25) Matsen, M. W.; Griffiths, G. H. *Eur. Phys. J. E: Soft Matter Biol. Phys.* **2009**, *29*, 219.
(26) O'Driscoll, B. M. D.; Griffiths, G. H.; Matsen, M. W.; Perrier, S. b.; Ladmiral, V.; Hamley, I. W. *Macromolecules* **2010**, *43*, 8177.
(27) Zhulina, E.; Balazs, A. C. *Macromolecules* **1996**, *29*, 2667.
(28) Zhulina, E. B.; Singh, C.; Balazs, A. C. *Macromolecules* **1996**, *29*, 6338.
(29) Zhulina, E. B.; Singh, C.; Balazs, A. C. *Macromolecules* **1996**, *29*, 8254.
(30) Tuteja, A.; Choi, W.; Ma, M.; Mabry, J. M.; Mazzella, S. A.; Rutledge, G. C.; McKinley, G. H.; Cohen, R. E. *Science* **2007**, *318*, 1618.
(31) Mabry, J. M.; Vij, A.; Iacono, S. T.; Viers, B. D. *Angew. Chem., Int. Ed.* **2008**, *47*, 4137.
(32) Ramirez, S. M.; Diaz, Y. J.; Campos, R.; Stone, R. L.; Haddad, T. S.; Mabry, J. M. *J. Am. Chem. Soc.* **2011**, *133*, 20084.
(33) Krishnan, S.; Kwark, Y. J.; Ober, C. K. *Chem. Rec.* **2004**, *4*, 315.
(34) Corpart, J.-M.; Girault, S.; Juhue, D. *Langmuir* **2001**, *17*, 7237.
(35) Honda, K.; Morita, M.; Otsuka, H.; Takahara, A. *Macromolecules* **2005**, *38*, 5699.
(36) Bunn, C. W.; Howells, E. R. *Nature* **1954**, *174*, 549.
(37) Honda, K.; Morita, M.; Sakata, O.; Sasaki, S.; Takahara, A. *Macromolecules* **2010**, *43*, 454.
(38) Niu, H.; Wang, F.; Weiss, R. A. *Macromolecules* **2015**, *48*, 645.
(39) Trent, J. S.; Scheinbeim, J. I.; Couchman, P. R. *Macromolecules* **1983**, *16*, 589.
(40) Bates, F. S. *Science* **1991**, *251*, 898.
(41) Bates, F. S.; Fredrickson, G. H. *Annu. Rev. Phys. Chem.* **1990**, *41*, 525.
(42) Zhu, L.; Cheng, S. Z. D.; Calhoun, B. H.; Ge, Q.; Quirk, R. P.; Thomas, E. L.; Hsiao, B. S.; Yeh, F.; Lotz, B. *Polymer* **2001**, *42*, 5829.
(43) Zhu, L.; Chen, Y.; Zhang, A.; Calhoun, B. H.; Chun, M.; Quirk, R. P.; Cheng, S. Z. D. *Phys. Rev. B: Condens. Matter Mater. Phys.* **1999**, *60*, 10022.
(44) Matsushita, Y.; Mori, K.; Saguchi, R.; Nakao, Y.; Noda, I.; Nagasawa, M. *Macromolecules* **1990**, *23*, 4313.
(45) Chen, W.; Zheng, J.; Cheng, S. Z. D.; Li, C.; Huang, P.; Zhu, L.; Xiong, H.; Ge, Q.; Guo, Y.; Quirk, R.; Lotz, B.; Deng, L.; Wu, C.; Thomas, E. *Phys. Rev. Lett.* **2004**, *93*, 028301.
(46) Zheng, J. X.; Xiong, H.; Chen, W. Y.; Lee, K.; Van Horn, R. M.; Quirk, R. P.; Lotz, B.; Thomas, E. L.; Shi, A.-C.; Cheng, S. Z. D. *Macromolecules* **2006**, *39*, 641.
(47) Bates, F. S.; Fredrickson, G. H. *Phys. Today* **1999**, *52*, 32.
(48) Alexander, S. *J. Phys. (Paris)* **1977**, *38*, 983.
(49) de Gennes, P. G. *Macromolecules* **1980**, *13*, 1069.
(50) Cantor, R. *Macromolecules* **1981**, *14*, 1186.
(51) Flory, P. J. *Principles of Polymer Chemistry*; Cornell University Press: Ithaca, NY, 1981.
(52) Ha, B.-Y.; Jung, Y. *Soft Matter* **2015**, *11*, 2333.
(53) Beckingham, B. S.; Register, R. A. *Macromolecules* **2013**, *46*, 3486.

DOI: 10.1021/acs.macromol.5b01661
Macromolecules 2015, 48, 7172−7179